



Investigating the influence of rotational speed in wire electric discharge machining of cylindrical workpieces: an experimental and simulation study

Jahangir Khosravi^{1,2} · Hamid Hesni³ · Bahman Azarhoushang^{1,2}

Received: 27 February 2024 / Accepted: 22 May 2024 / Published online: 4 June 2024
© The Author(s), under exclusive licence to Springer-Verlag London Ltd., part of Springer Nature 2024

Abstract

Wire electrical discharge machining (WEDM) is a non-conventional machining process renowned for precision in machining complex profiles, especially in high-strength and hard materials. This process also found other functions in machining cylindrical workpieces, known as wire electrical discharge turning (WEDT). The material removal mechanism of this process is based on electrical discharges, and evaluating the productivity of the continuous process to a great extent depends on the material removal of individual single discharges. In order to study the influence of rotational speed in material removal of erosion in cylindrical workpieces, theoretical and experimental studies of each single spark are necessary. This comprehensive study delves into the influence of rotational speed in WEDM processes applied to cylindrical workpieces. The research includes a series of single discharge experiments, and introduces a computational fluid dynamics (CFD) thermal model. The developed thermal model demonstrates the capability to predict the material removal rate of a single discharge with an error of 8.6% relative to experimental data. Furthermore, the investigation extends to continuous erosion studies, analyzing the material removal rate under varying rotational speeds. The overall material removal rate decreases 13% due to the declining material removal rate of each single discharge. Additionally, a removal efficiency parameter of erosion of cylindrical workpieces is introduced to provide an evaluation of the process and the influence of crater overlaps. The removal efficiency for various rotational speeds ranges between 22 and 24%, influenced by the proportion of normal discharges and the efficiency of crater overlaps.

Keywords Wire electric discharge machining · Thermal model · Simulation · Single discharge · Wire electric discharge turning · CFD simulation

1 Introduction

Wire electrical discharge machining (WEDM) is a non-conventional machining process known for its high precision and capability to produce complex forms, even in high-strength, high hardness, and difficult-to-cut materials [1, 2]. The material removal mechanism in this process is similar to electrical discharge machining (EDM), which is

rooted in generating discharges between the wire and workpiece in a dielectric medium, which generates craters on the workpiece surface on the microscale. This electro-thermal process involves discrete electrical sparks, creating a high-temperature plasma channel that erodes the workpiece material through local melting and vaporization [3]. The accumulation of successive craters contributes to the gradual erosion of material. Although thermal energy was applied to the workpiece for material removal, high-frequency discharges allow for the fabrication of parts with minimal thermal damage [4]. Understanding the fundamental procedures of EDM is crucial for pushing productivity boundaries, involving investigations into both continuous erosion processes and the analysis of single discharges [3]. In this context, experimental studies have delved into the efficiency of pulses in continuous WEDM by focusing on the influence of individual WEDM parameters on material removal during

✉ Bahman Azarhoushang
bahman.azarhoushang@tf-pr.uni-freiburg.de

¹ Institute for Advanced Manufacturing (KSF), Furtwangen University, Tuttlingen, Germany

² Department of Microsystems Engineering (IMTEK), University of Freiburg, Freiburg, Germany

³ Senergie Technologies GmbH, Engen, Germany

single discharges [1, 5]. Given the fundamental role of each discharge in the process, developing a comprehensive model for a single discharge is crucial for understanding the process and parameters that influence the removal rate [1, 3, 6, 7].

The modeling of single discharges in EDM is challenging due to the incomplete understanding of the underlying physics. A comprehensive clarification of the EDM process requires an investigation of various aspects such as thermodynamics, electrodynamics, and hydrodynamics [1]. The simulation of the material removal rate (MRR) in the EDM process typically relies on an electro-thermal model. Because the material is removed due to the high temperatures during discharge attained in the plasma channel [8]. Since the 1970s, various attempts have been made to simulate the single discharge of EDM with different assumptions, considering the volume of material exceeding the melting temperature is removed [9]. In most modeling approaches, the temperature distribution within the workpiece is calculated based on a non-uniform Gaussian distribution of heat flux [3, 7, 10]. Further developments in thermal modeling include considerations on the efficiency of growth of discharge radius, the temperature dependence of material properties, and the latent heat of fusion [11]. Assarzadeh and Ghoreishi [3] conducted a study on the electro-thermal simulation and experimental validation of material removal in EDM. They introduced more realistic conditions such as a Gaussian-type distribution of spark heat flux, temperature-dependent material properties, latent heat of melting, and an expanding plasma channel. The finite element method (FEM) was employed for simulation to simulate MRR of the process. Lower confirmation errors in crater radius and depth were achieved compared to previous thermal models.

Each individual discharge in the EDM process occurs within a very short period, lasting only a few microseconds. This short duration poses a challenge in constructing a comprehensive model for predicting material removal during the process. In the context of WEDM processes, this duration is further diminished to less than 5 μ s type of generator used. The reduction in pulse on-time contributes to the complexity of simulating the process, which needs some considerations [12]. Wang et al. [7, 11] investigated the crater volume in WEDM through experimental and numerical study. The thermal model presented, incorporating a temperature-dependent equation for plasma channel radius increase, establishes a correlation with actual MRR, demonstrating deviations below 10%. The assumptions are based on the radially symmetric crater in the mentioned model and some other existing models. However, based on observations, it is noted that this does not accurately reflect the real shape of a single crater in WEDM. The actual crater form of single discharges in WEDM is asymmetric. The craters' elongation results from the wire geometry's influence on the process. As the plasma grows, it

becomes constrained by the wire geometry after reaching a certain energy level [1]. Incorporating this condition into a thermal model could lead to an improvement in model accuracy.

WEDM offers another function by incorporating a rotary spindle into the machine table for eroding cylindrical parts. This specific application is wire electrical discharge turning (WEDT) [13, 14]. Furthermore, the application of this process also extends to the conditioning of grinding wheels with electrically conductive bonds, termed wire electric discharge conditioning (WEDC) [15–17]. In the mentioned applications, the rotation speed of the spindle, along with other WEDM parameters, plays a crucial role. However, the available research on the influence of spindle speed on the removal rate during erosion is limited and, in some instances, shows significant variation [18, 19]. Uhlmann et al. [19] studied the influence of rotational speed in the micro-WEDT of cylindrical parts. They found that at low discharge energies, the rotation of the workpiece reduces the removal rate. This reduction is attributed to the effectiveness of flushing effects in the presence of rotation. Also, they mentioned that a high removal rate is achievable at higher discharge energies with increased speed. Weingärtner et al. [18] found that high relative speeds, reaching up to 80 m/s, can enhance the material removal during WEDC, because at higher relative speeds, the plasma channel slides on the material during on-time. This allows the discharge energy to be more efficiently utilized for melting additional material rather than merely causing overheating in the melting pool.

According to the current state of the art, there is potential to investigate the material removal in the erosion of cylindrical parts through individual discharge experiments and simulations. Also, it is worth highlighting that there is currently no reported study on the influence of rotational speed, specifically on a water-bath WEDM machine for bronze material. This study aims to experimentally study the material removal of single WEDM discharges on cylindrical parts with different rotational speeds. The experiments are designed to study the dimensions of craters and the volume of each crater performed by one single discharge. Furthermore, a computational fluid dynamics (CFD) thermal model is developed and verified with experiments. In this model, not only are temperature-dependent material properties and plasma channel sliding (because of the rotation of the workpiece) considered, but they also account for the crater's asymmetric form and the dielectric's cooling effect. Lastly, the material removal rate during continuous erosion under various rotational speeds was investigated, and the results were compared with the results of single discharge experiments. In this part of the study, the efficiency of discharges and the overlapping influences of craters were thoroughly examined. The outcomes of this study could lead to the scientific approach to efficiently conditioning grinding wheels

with metal-bonded materials, typically found in close proximity to the materials investigated in this study.

2 Concept and boundary condition of numerical simulation of WEDM

In order to investigate the correlation between material removal in single discharges and the continuous WEDM process, a thermal model for single discharges was developed using CFD. Previous researches relied on finite element analysis (FEA) simulations, where the heat transfer coefficient is unknown [20]. However, in the present method, the heat transfer coefficient can be accurately calculated transiently using CFD equations at any velocity of the medium. Another notable advantage of applying the CFD method is that the heat source and all its parameters can be parametrized. This capability is crucial for expanding the radius of heat flux and tracking the movement of the heat flux during the discharge time.

Existing models, rooted in classical Fourier heat conduction theory, typically assumed that heat distribution on the surface of the workpiece follows a Gaussian distribution. To model the transmission of heat received by the workpiece during a single discharge, the Fourier heat conduction equation (Eq. (1)) is solved. In this equation, T represents temperature, X , Y , and Z denote distances from the center of heat flux in the Cartesian Coordinate System, ρ is the density, t is the time, C_p is the specific heat, and K is the thermal conductivity.

$$\frac{\partial}{\partial x} \left(K_x \frac{\partial T}{\partial x} \right) + \frac{\partial}{\partial y} \left(K_y \frac{\partial T}{\partial y} \right) + \frac{\partial}{\partial z} \left(K_z \frac{\partial T}{\partial z} \right) = \rho C_p \frac{\partial T}{\partial t} \quad (1)$$

In this model, the thermal energy applied to the workpiece is represented as a Gaussian heat flux, consistent with expressions found in other studies and described by Eq. (2) [3]. Given that, the plasma channel radius (R_p) expands with pulse on-time, and F_c represents the fracture factor introducing the actual fraction of energy to the workpiece. Additionally, V and I denote the voltage and current of the discharge, measured during the process, while r signifies the radial position of the heat flux. This formula is widely employed by researchers in the field of sinking EDM as well as wire EDM [3]. As evident, the heat flux distribution exhibits a symmetrical shape. In the initial phase of this article, this form of heat flux is utilized to simulate the EDM single spark. For the subsequent phase, a novel elliptical Gaussian heat flux is developed and implemented to simulate the wire EDM single spark with an elliptical shape (Eq. (3)). In this equation, plasma channel radius in the Y -axis direction which is perpendicular to wire direction (R_{py}) is equal to

R_p , and plasma channel radius in the X -axis direction and perpendicular to wire direction (R_{px}) is equal to “elliptical aspect ratio * R_{py} .”

$$Q(r) = \frac{4.57 F_c VI}{\pi R_p^2} \exp\left(-4.5 \frac{r^2}{R_p^2}\right) \quad (2)$$

$$Q(x, y) = \frac{4.57 F_c VI}{\pi R_{px} R_{py}} \exp\left(-4.5 \left(\frac{x^2}{R_{px}^2} + \frac{y^2}{R_{py}^2}\right)\right) \quad (3)$$

The plasma radius is a critical parameter influencing both the geometry of discharge craters and the temperature distribution. This parameter depends on various factors such as electrode (wire) and workpiece material, pulse energy, and dielectric and the shape of the electrode. Researchers have proposed numerous approaches to formulate equations for plasma radius (R_p). This study employs a radius equation that has been proven effective for short on-time discharges during WEDM and has resulted in accurate models (Eq. (4)) [11]. Literature indicates that single discharge craters exhibit asymmetry based on experimental results. To enhance the prediction accuracy of the model, a 3D model is introduced to simulate asymmetric craters. Achieving an elliptical shape for the crater, instead of a circle, involves increasing the growing speed of the discharge in the length direction, guided by the aspect ratio of the crater observed in experiments.

$$R_p = (2e - 5) + 30.5t \quad (4)$$

As boundary conditions for the simulation, the workpiece is placed in a water tank. To approach to real condition, a user-defined water specification is employed. This specification ensures that, after reaching a temperature of 100 °C, crucial parameters such as density, specific heat (C_p), thermal conductivity, and dynamic viscosity undergo changes to match the properties of steam. Because, by raising the water temperature during discharge, water boils, and the medium in contact with the high-temperature workpiece transitions to steam. Initially, water convection is applied in the simulation on the workpiece surface. As time progresses and the water temperature rises, air convection becomes applicable in the simulation. Depending on the rotational speed of the workpiece in the experiment, the water flows at a linear speed corresponding to the rotational speed of the workpiece. To incorporate the influence of the workpiece’s rotational speed, the heat flux is moved with a linear speed along the workpiece surface at the same rate as the rotation.

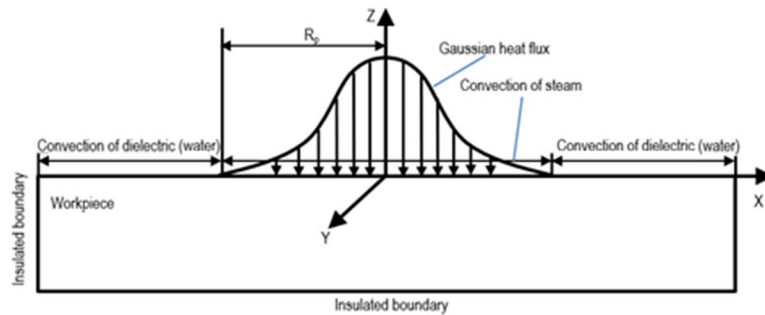
In WEDM, material removal occurs through the phenomena of melting and vaporization. During the melting and vaporization of the material, energy is absorbed by the workpiece without changing its temperature. To

improve the accuracy of the simulation, considering the effect of latent heat is suggested. In this study, the influence of fusion latent heat is taken into account to enhance the correlation with experimental results but the vaporization latent heat has been neglected. The effective heat capacity method (EHCM) is employed for melting model as it is shown in Eq. (5).

$$C_p(T) = C_p(t) = \begin{cases} C_{p, solid} & T < T_m \\ \frac{L}{T_s - T_m} + C_p(T) & T_m \leq T \leq T_s \\ C_{p, liquid} & T > T_s \end{cases} \quad (5)$$

where T_m is the melting (liquidus) temperature, T_s is the solidification (solidus) temperature, and L is the fusion latent heat [21]. Furthermore, the material properties undergo changes based on temperature variations. In this work, all material properties (except density of workpiece) are considered to be temperature-dependent. Also, the parameters of the CFD analysis and a schematic representation of the finite element analysis are also shown in Fig. 1.

Fig. 1 The schematic drawing of CFD analysis and related parameters



3 Experimental setup

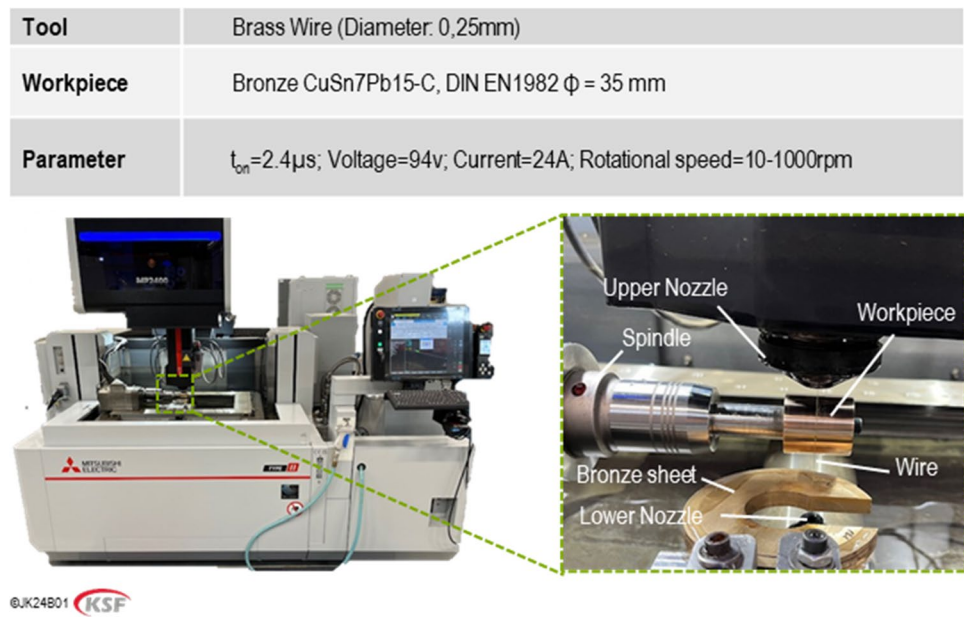
To conduct the experiments, well-polished bronze CuSn7Pb15-C, DIN EN1982 material with a diameter of 35 mm was employed to perform single discharges and continues eroding process. This material was selected as a representative of bond material in metal-bonded grinding wheels. A water-based WEDM machine manufactured by Mitsubishi Electric (MP2400 precision series) equipped with an additional rotary spindle (ITS Technologies RSI-55) was employed to perform the experiments with a brass wire of diameter 0.25 mm. Due to the specifications of the generator, a bronze material sheet is simultaneously cut during the single discharge test to ensure the stability and separation of individual discharges. The WEDC setup and corresponding parameters are shown in Fig. 2 The current, discharge voltage, and pulse on time were measured by a 2 Channel Digital Storage Oscilloscope TBS1052C.

As shown in Fig. 3, the single discharge experiments were executed employing two different strategies. The first strategy (Fig. 3a) involves the single discharge using the tip

Parameter	Description
Material of Fluid	Water, Temperature dependent
Material of Workpiece	Bronze ; CuSn7Pb15-C, DIN EN1982, Temperature dependent
Initial temperature of water , T	17.0°C
Radius of the cylindrical workpiece	250.0µm
Height of Cylindrical Workpiece	200.0µm
Time of solution, t	2.4µs
Workpiece density , ρ	9200kg/m ³
Specific heat capacity of workpiece , C _p	Temperature dependent J/Kg.K
Discharge current, I	24.0 A
Pulse on-time , t _{on}	2.4 µs
Fraction factor for elliptical heat gaussian flux, F _c	0.6
Fraction factor or cylindrical heat gaussian flux, F _c	0.4
Gap Voltage , V	94.0v

©JK24B14 KSF

Fig. 2 The machine setup of WEDM and the process parameters



of a sharpened section of a 0.25-mm brass wire. Despite the cylindrical shape of the workpiece, this method results in a radially symmetric crater form. The second strategy (Fig. 3b) involves performing single discharges using the cylindrical area of the wire, representing the actual erosion process of a WEDM process. Even with similar parameters, this method yields an elliptical crater form when viewed in Fig. 3a. As discussed in the literature review, this phenomenon is attributed to the difference in electrode form and the elongation of the plasma channel in the wire direction. Both strategies are chosen for conducting single discharges to ensure accurate assumptions in the single discharge study. The craters that resulted in single discharges were assessed by measuring the depth, diameter, and volume of the single craters. To achieve this objective, optical microscopy (KEYENCE, VHX 5000) is employed.

Also, the MRR in continuous WEDM on cylindrical workpieces based on single discharges was studied. A cylindrical bronze workpiece is eroded at different rotational speeds, and the eroding time of the process under an adaptive control feed rate is recorded to examine the material removal from the workpiece. The feed rate was set by the adaptive control feature of the machine generator to achieve the highest possible MRR with the established process parameters. The same parameters as for the single discharges are utilized here. Figure 4 shows schematically the experimental setup for continuous eroding of the workpiece. The depth of cut was 0.3 mm, and the rotational speeds ranging from 200 to 1000 rpm were used, at the same intervals as in the single discharge test. The continuous test at 10 rpm could not be carried out due to the wire breakage. Further, WEDC parameters like wire tension, speed, and flushing amount were kept constant.

4 Results and discussions

4.1 Thermal modeling of WEDM

The thermal model employed for the radially symmetric single discharge is based on the method outlined in Fig. 3a and utilizes the heat flux growth equation (Eq. (3)). This model incorporates temperature-dependent material properties, fusion latent heat of workpiece, transient convection of fluid, and changing properties of the water as dielectric to steam. For this model, the bronze alloy material CuSn7Pb15-C was chosen, with a melting point of 900 °C and solidus point 820 °C and a fusion latent heat of 170 kJ/mol. According to existing literature, the F_c parameter in simulations is commonly assumed to fall within the range of 14 to 50% [22]. Given that a value of 40% for F_c has demonstrated a strong correlation with results in WEDM simulations [7], this study adopts the same setting for F_c to ensure a reliable and consistent representation of the process. Figure 5 depicts temperature distribution contours and molten pool profile after a 2.4- μs discharge, revealing the formation of a circular crater. The molten pool profile indicates that the material's temperature exceeds the melting point of bronze, where the required fusion latent heat is absorbed by the material. The parameters h , d_a , and d_b respectively denote the maximum depth of the crater and the diameters of the crater in the X and Y directions. According to this simulation, the diameter of the crater induced by a single spark is 130.6 μm (d_a/d_b), and the maximum depth of the crater is 11.62 μm (h). These dimensions result in a crater with a volume of 45,423 μm^3 . Since the recast layer in this process is thinner than a few microns, it can be assumed that 100% of melting pool is being removed during discharge.

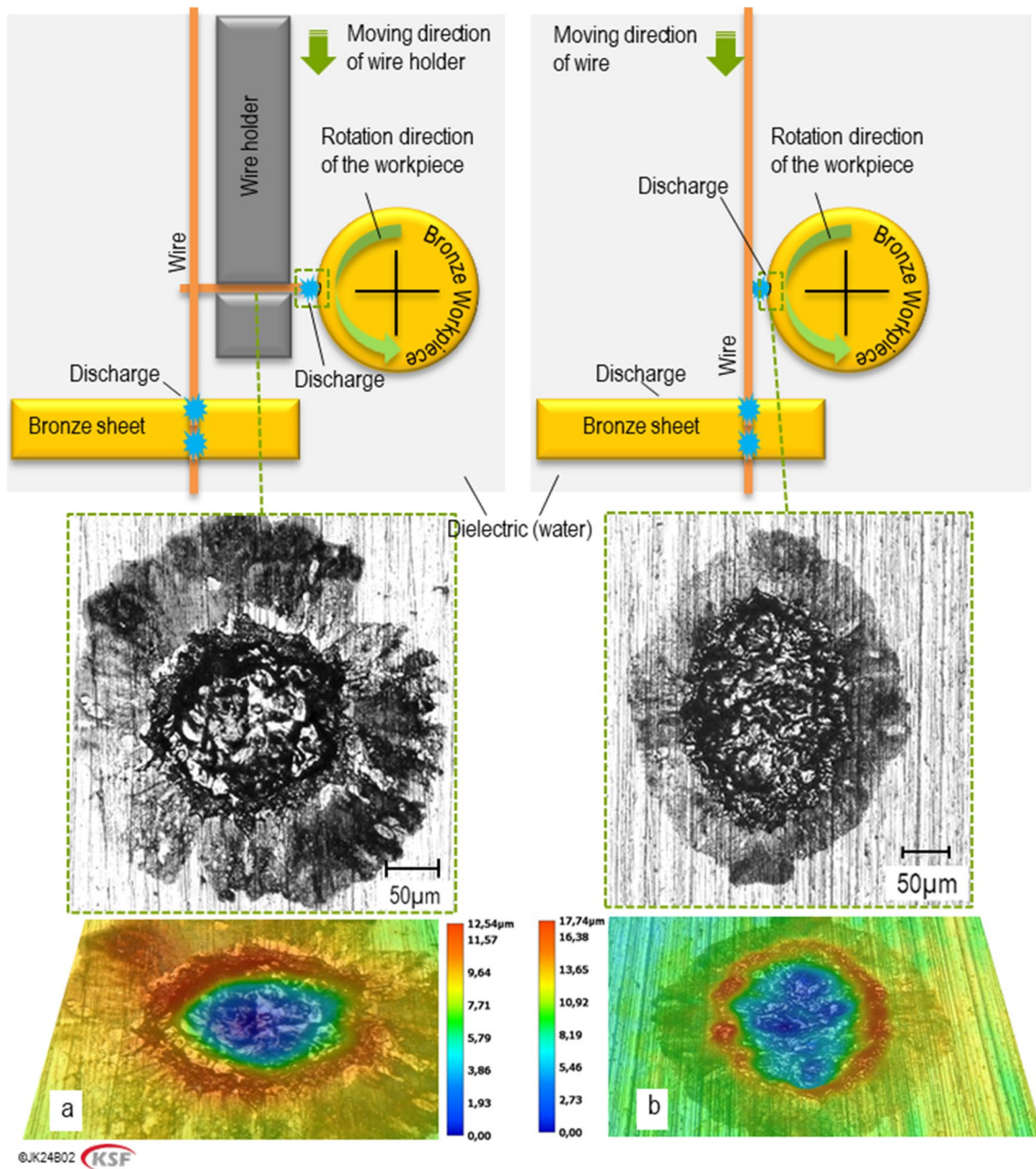


Fig. 3 Schematic illustration of the WEDM single discharges on the cylindrical workpiece and optical microscopy image of the single discharge performed by **a** the sharp tip of a wire electrode section and **b** the cylindrical surface of the wire area

Figure 6 shows the temperature trend of the middle point of the plasma channel applied to the workpiece during the discharge time (time-on). It is evident that the temperature undergoes a rapid and sharp increase immediately after the discharge initiation. The temperature theoretically reaches $75,900\text{ }^{\circ}\text{C}$ just $0.3\text{ }\mu\text{s}$ after the start of the discharge, a phenomenon attributed to the instantaneous behavior of heat flux. Subsequently, the temperature follows a continuous decreasing trend until the end of the discharge time.

In Fig. 7, an optical microscopy image along with the dimensions of a crater from a single discharge experiment is presented. A minimum rotational speed of 10 rpm was necessary to avoid overlapping of single discharges. The wire speed and rotational speed of the workpiece are of the same order and direction, making the experiment comparable with the simulation without considering the rotational speeds. The dimensions and volume of the crater resulting from a single discharge were compared with those predicted by the simulation. The simulated crater diameter and depth were

Fig. 4 Schematic view of the continuous material removal of a cylindrical workpiece in a WEDM machine

Parameter	ON-Time	Voltage	Current	Depth of cut	OFF-time	Rotational speed
Value	2,4µs	94V	24A	0,3mm	60µs	10-1000 rpm

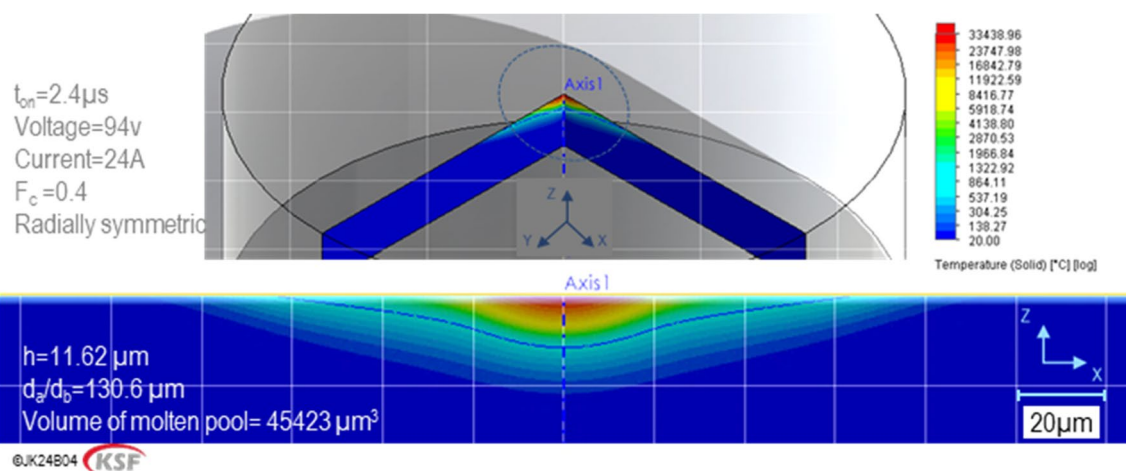
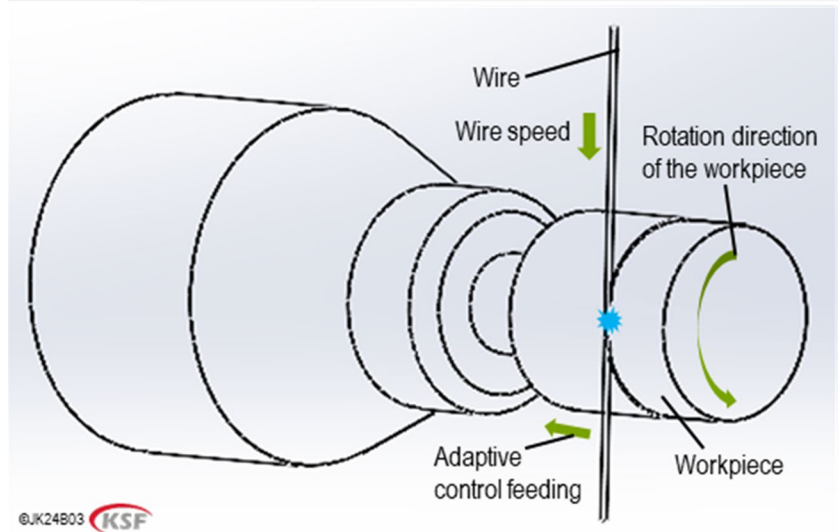


Fig. 5 Temperature distribution contours and molten pool profile of the developed thermal model with a radially symmetrical form

validated against experimental results with errors of 3.8% and 4.2%, respectively. Also, the thermal model simulates the single discharge process with a 4.6% error in material removal compared to the experiment. It is important to note that material removal in both the experiment and the model is considered without accounting for the rim created around the crater.

Many available simulations often rely on simplifications that can impact the accuracy of the simulation results. Figure 8 illustrates the influence of time-dependent material properties and fusion latent heat on the assumption accuracy of our model. As depicted in Fig. 8, simplifying the model by neglecting fusion latent heat and temperature-dependent

material properties (profile c) results in a significantly larger crater, with the depth of the molten pool increasing to 21.25 µm, which is 190% deeper than the real value (profile a). Conversely, by incorporating temperature-dependent material properties, the depth of the molten pool decreases to 17.45 µm (profile b), as the energy associated with phase changes presents additional resistance to the heat penetrating the material. Nevertheless, this is still 156% larger than the model considering latent heat. Although dielectric convection has been applied to improve model accuracy, its influence on crater size is minimal.

The model presented above focuses on a radially symmetric single discharge, which does not accurately represent

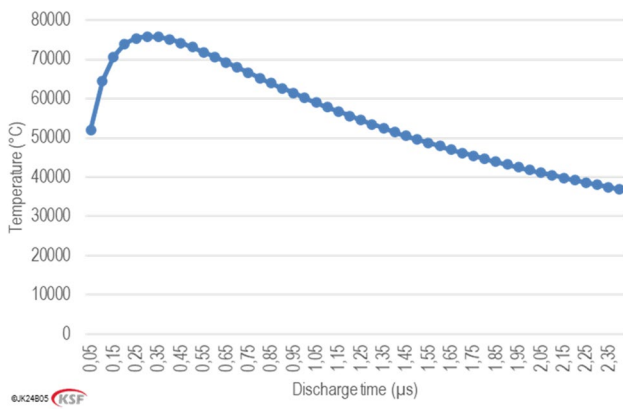


Fig. 6 Temperature of the middle point of the plasma channel ($I=24$ A, $t_{on}=2.4 \mu\text{s}$, and $V=94$ V)

and describe the real discharge of the WEDM process. As mentioned in the state of art, the actual form of the single discharge (depending on the discharge energy) is elliptical. Therefore, to comprehensively study the WEDM process based on single discharges, it is crucial to consider actual single discharges, as depicted in Fig. 3b. This type of single discharge is elliptical, necessitating the modeling of different growth of heat flux in the X and Y directions. In Fig. 8, optical microscopy images and dimensions of the crater section resulting from a single discharge experiment are presented.

Fig. 7 An optical microscopy image and dimensions of a single discharge experiment induced by the method introduced in Fig. 3a

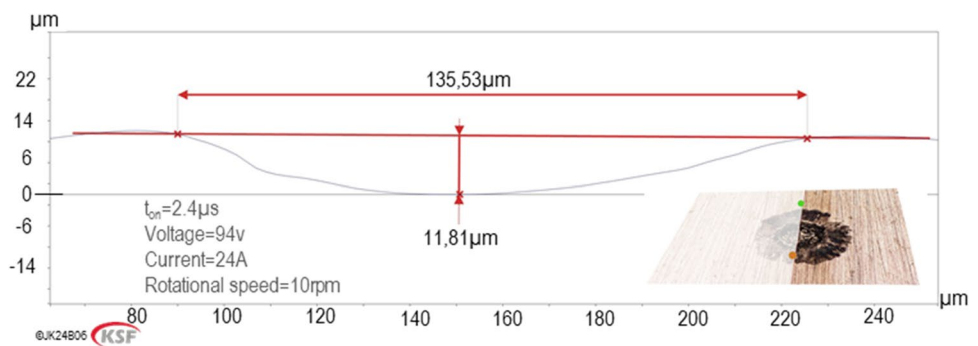
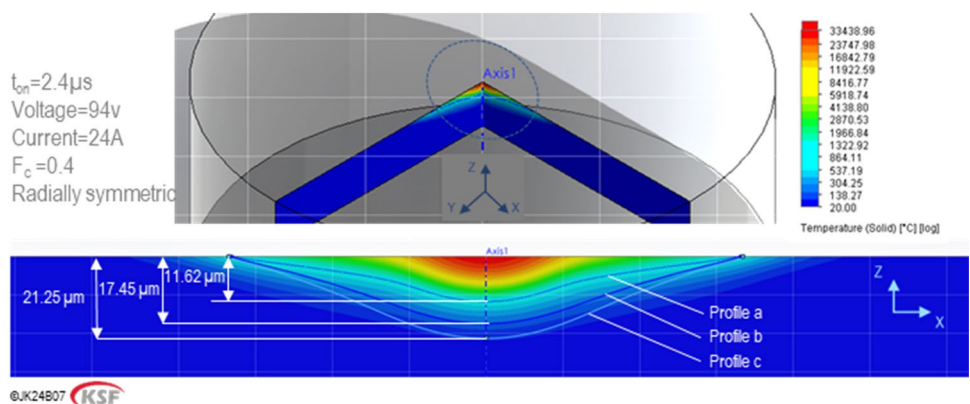


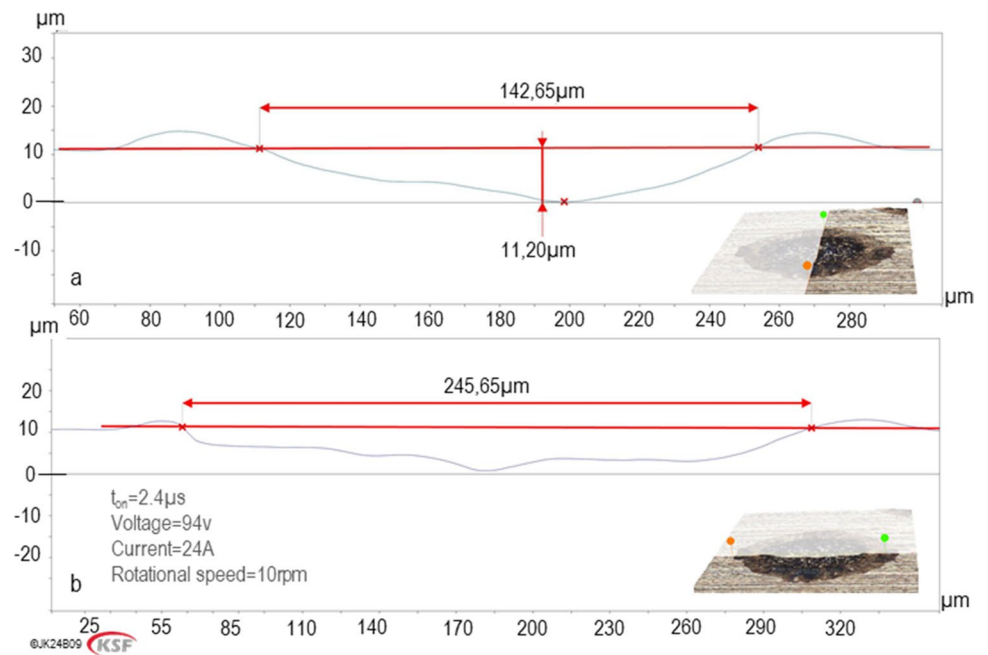
Fig. 8 Comparison of the molten pool profile in the thermal model: (a) considering the temperature-dependent material properties and the latent heat of fusion; (b) with the simplified model without considering the latent heat of fusion; (c) with the simplified model without considering temperature-dependent material properties and the latent heat of fusion



The single discharge was conducted using the method depicted in Fig. 3b, closely resembling the actual material removal scenario in the erosion of cylindrical workpieces in a WEDM machine. As observed in Fig. 9a and b, the larger axis of the crater ellipse is elongated in the wire direction, aligning with the elongation of the plasma channel with a diameter ratio of 1.8.

In simulation of elliptical form of single discharge, the elongation ratio is derived from single discharge experiments and applied to the thermal model's heat flux growth (Eq. (4)). Consequently, the diameter ratio of 1.8 (X to Y direction) for the elliptical form of the crater from the experiment is applied in the heat flux equation. X is the direction of the crater parallel to the wire direction and Y is the direction along with the lateral direction and perpendicular to the wire direction. All other factors except fraction factor (F_c) are considered similar to the model in Fig. 5. With this new elliptical Gaussian heat flux, it is observed that to reach an accurate shape of molten pool corresponding to experiment the F_c must be increased to 60%. The increase in the fraction factor can be attributed to the shape of the wire, wherein a larger fraction of the total heat is absorbed by the workpiece. In simpler terms, the size and shape of the crater are influenced by the shape of the wire, in addition to all other previously known parameters. As a result, the single discharge is modeled with an elliptical form, and the dimensions of the crater based on the temperature distribution contours

Fig. 9 Optical microscopy images and dimensions of single discharge experiment induced by the method introduced in Fig. 3b with elliptical form: **a** elongated in the wire direction and **b** perpendicular to wire direction

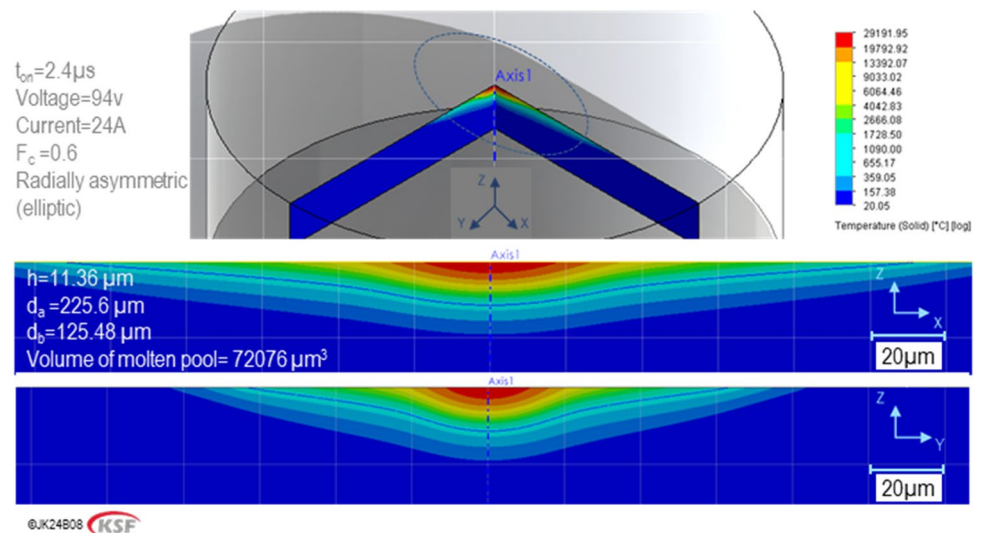


and molten pool profile are illustrated in Fig. 10. According to this simulation, the diameter of the crater induced by a single spark has a large diameter of 225.6 μm (d_a) and a minor diameter of 125.48 μm (d_b), with the maximum depth of the crater measuring 11.36 μm (h). These dimensions collectively result in a crater with a volume of 72,076 μm^3 . The validation of the model and experiment shows that the model can predict material removal with an 8.6% error. Also, the simulated crater diameter in large and small diameter and depth was validated against experimental results with errors of 8.16%, 12%, and 1.4%, respectively. It is notable that in the vicinity of the crater, a rim is formed primarily due to the recasting of molten pool which is not considered in calculations as well.

4.2 Single discharges considering rotation speed

The measurements of the craters, as depicted in Fig. 11, reveal that the increase in rotational speed from 10 to 200 rpm (0.02 to 0.37 m/s) has a minimal influence on the material removal of the single discharge. However, with further increases in rotational speeds up to 1000 rpm (1.83 m/s), the material removal of a single discharge decreases. Previous studies have mentioned that parameters influencing material removal at different speeds include increased heat transfer and the influence of plasma sliding [6, 19]. The former generally leads to a decrease in the material removal rate. The second phenomenon is claimed to cause an increase in the MRR. The influence of both factors

Fig. 10 Temperature distribution contours and molten pool profile of the developed thermal model with an elliptical form (asymmetrical)



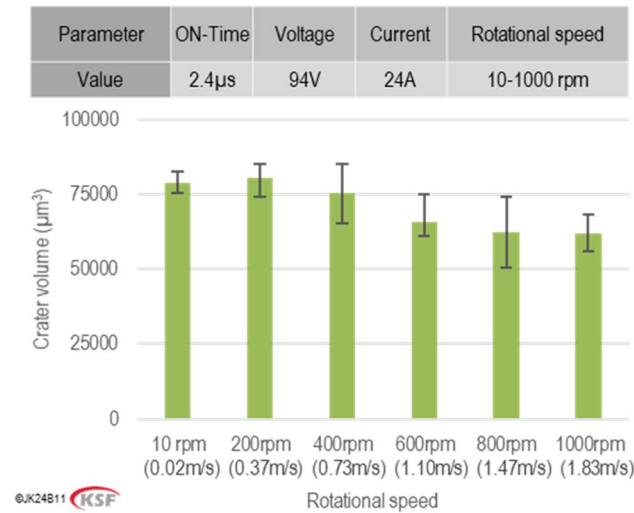


Fig. 11 Material removal volume of WEDM single discharges at different rotational speeds

is investigated by the thermal model, simulating the temperature distribution of the discharge up to a rotational speed of 1000 rpm (1.83 m/s), where sliding of the plasma on the material surface and the flow of dielectric on the workpiece’s surface occur.

Figure 12 shows the profile of the crater in the thermal model of a single discharge at different rotational speeds. The simulation of a single discharge crater with a rotation of 1000 rpm (1.83 m/s) indicates that the center of the simulated single discharge is displaced due to the relative transversal speed of the heat flux and the workpiece. On one hand, comparing the middle section of the crater reveals that the crater’s form is influenced by the sliding of the plasma channel on the

workpiece, differing from the simulated crater without considering rotational speed. On the other hand, the influence of dielectric convection is very low at 1000 rpm rotation (Fig. 12b), evident in both the depth and diameter of the crater. Overall, the area of the crater is decreased, but the change is negligible. This trend differs from the experimental results shown in Fig. 11. Phenomena such as turbulence and wire vibration, which are not considered in the simulation, could impact the process by decreasing F_c at higher rotational speeds and cause lower material removal in experiments. The maximum rotational speed in these experiments is 1000 rpm; however, to demonstrate the influence of rotational speed in a higher range, as mentioned in Wegener’s study [18], a rotational speed of 20 m/s is applied in the simulation. The results indicate that this high rotational speed range theoretically increases the removal rate (Fig. 12c). Figure 13 provides a summary of the comparison between the experimental values of material removal for each spark and the simulation results.

4.3 Continues eroding of cylindrical workpiece

The material removal rate during the continuous erosion of a cylindrical workpiece is investigated through experiments. The MRR of the process is calculated using Eq. (6), where r_w represents the radius of the workpiece, d is the depth of cut, b is the width of removed material in the axis direction, and t_p is the process time.

$$MRR = \frac{\pi * b * (r_w^2 - (r_w - d)^2)}{t_p} \tag{6}$$

Figure 14 presents a comparison of the MRR during continuous erosion at different rotational speeds. Initially,

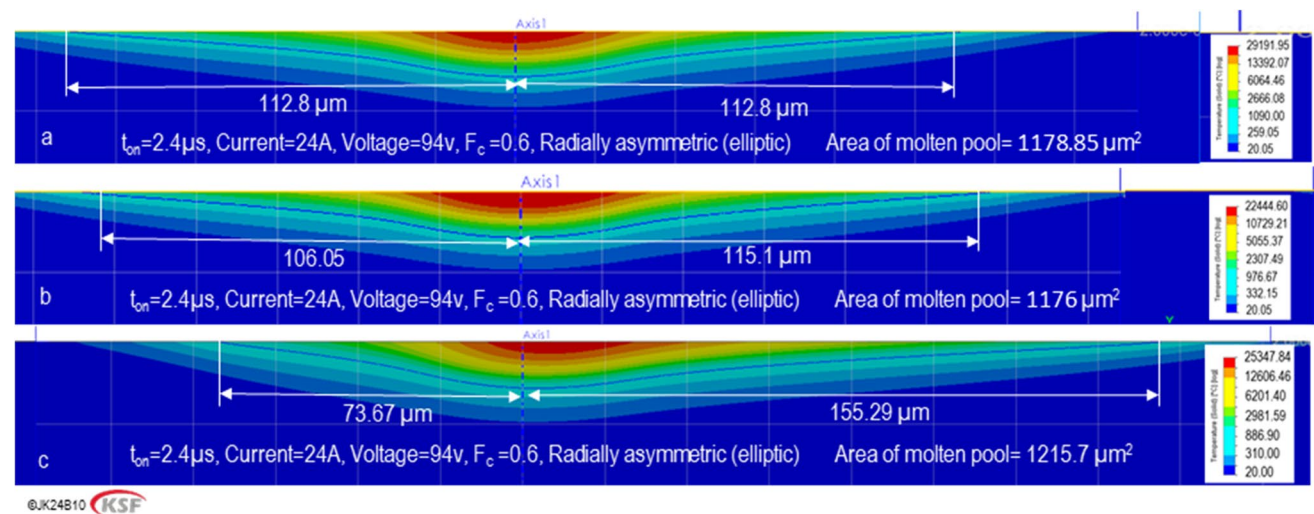


Fig. 12 Comparison of the temperature distribution contours of the molten pool profile in the developed thermal model: **a** without rotational speed; **b** with 1000 rpm (1.83 m/s) rotational speed of the workpiece; **c** with 11,000 rpm (20 m/s) rotational speed of the workpiece

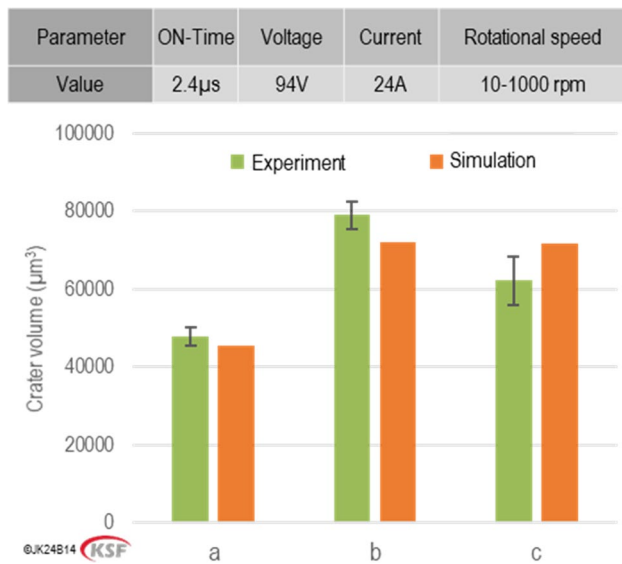


Fig. 13 Comparison of the material removal volume of WEDM single discharges in experiment with simulation: (a) radially symmetric crater without rotational speed; (b) elliptical crater without rotational speed; (c) elliptical crater with 1000 rpm (1.83 m/s) rotational speed of the workpiece

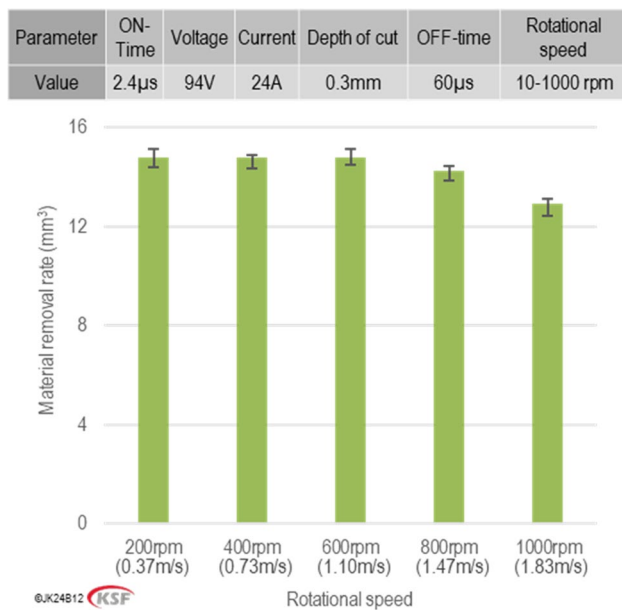


Fig. 14 Material removal of the continuous WEDM at different rotational speeds

no significant impact is observed as the rotational speed increases from 200 to 600 rpm. However, as the rotational speed is further increased to 800 and 1000 rpm, the MRR

exhibits a negative trend. This aligns with observations in single discharges, where the material removal of each individual discharge gradually decreases with an increase in rotational speed. This suggests that the overall material removal rate decreases due to the declining MRR of each single discharge. At lower rotational speeds, up to 600 rpm, the increase in rotational speed assists in moving debris away from the discharge zone by facilitating the flow of water around the workpiece. This effect can enhance the number of effective eroding pulses, preventing a decrease in the material removal rate within this rotational speed range. It is important to note that the flushing effect becomes less significant in the material removal of a single discharge, as the volume of debris in the dielectric is very low.

Welschof et al. [5] introduced a novel assessment characteristic for evaluating the continuous eroding process, termed removal efficiency, in cutting a workpiece using WEDM. This study introduces a new version of the removal efficiency (η_r) for the erosion of cylindrical workpieces, and the calculation is provided in Eqs. (7)–(9).

$$\eta_r = \frac{V_{w,eff}}{V_{w,theo}} \tag{7}$$

$$V_{w,eff} = \pi * b * (r_w^2 - (r_w - d)^2) \tag{8}$$

$$V_{w,theo} = V_{sing} * f_e \tag{9}$$

The effective material removal rate ($V_{w,eff}$) is determined by the actual material removal during continuous erosion, while $V_{w,theo}$ represents the material theoretically removed based on the material removal of each individual discharge (V_{sing}) and the discharge frequency (f_e). The removal efficiency (η_r) for various rotational speeds ranges between 22 and 24%. Two significant factors contribute to this phenomenon. Firstly, the proportion of normal discharges capable of efficiently removing material in different scales is crucial. The physical characteristics of the gap area can result in non-efficient discharges, reducing the overall removal efficiency of the process. Secondly, the efficiency of crater overlaps plays a role. Figure 15 shows the influence of crater overlaps, where Fig. 15a represents a crater caused by a single discharge on a polished surface, and Fig. 15b shows two craters with partial overlap. While it is theoretically expected that two consecutive discharges would remove twice the material, measurements indicate that this amount is 66.1% of the expected material removal. A similar analysis with three overlaps (Fig. 15c) shows a removal efficiency decrease of 48%. The combination of these two phenomena contributes to the observed low removal efficiency.

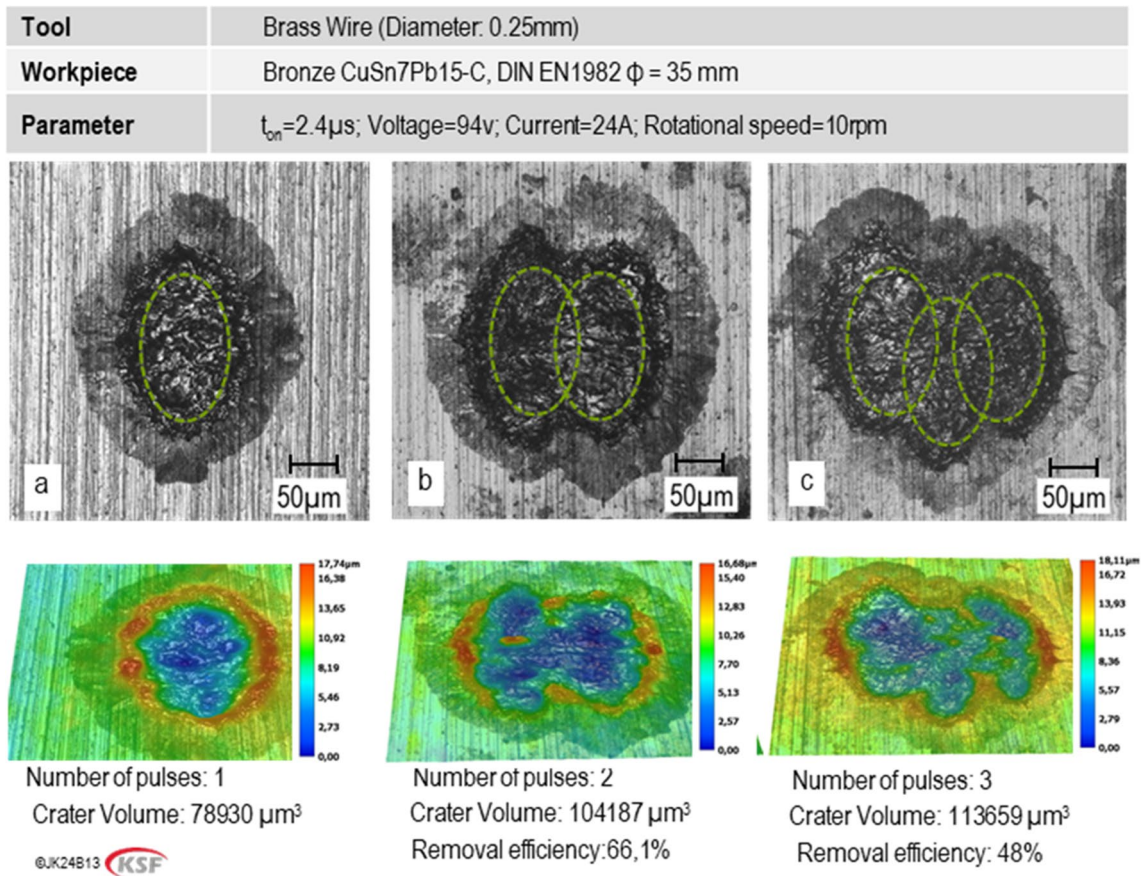


Fig. 15 Optical microscopy image of the WEDM single discharges on the bronze material: **a** one single sparks; **b** two single discharges with overlap; **c** three single discharges with overlaps

5 Conclusion

This study investigated the material removal of erosion in cylindrical workpieces made of brass based on simulation and experimental study of single discharges. Correspondingly, continuous erosion processes were performed to understand the influence of every single spark on material removal of a continuous process, and the following conclusions were made:

- The presented thermal model for single discharges is created based on the radially symmetric form of a crater. The model in this study was developed to simulate the actual form of single discharges with asymmetric forms. Validation against experiments with an error of 8.6% demonstrates promising results, which is crucial for understanding the material removal process.
- The experimental study reveals the influence of rotational speed on material removal in single discharges, indicating minimal effects at lower speeds and a diminishing trend to 21% at higher speeds. Simulating single discharges at higher available rotational speed assumes

that factors such as the sliding of the plasma channel and convection heat transfer do not significantly impact the material removal rate in the provided rotational speed range. However, in theory, increasing rotational speeds could enhance the material removal of the discharges in higher rotational speeds.

- The experiments to investigate continuous erosion conducted at various rotational speeds offer a comprehensive understanding of the continuous erosion process. The study reveals that, up to a certain rotational speed (600 rpm in this case), an increase in speed positively influences material removal, attributed to the enhanced flushing effect aiding in debris removal and promoting more effective eroding discharges. However, a diminishing trend up to 13% emerges beyond this threshold, indicating that the benefits of rotational speed start to decline. This diminishing effect is attributed to the declining material removal rate of each individual discharge at higher rotational speeds.
- Introducing removal efficiency as an assessment characteristic provides a comprehensive evaluation of discharge efficiency and the influence of crater overlaps. The efficiency of discharge is between 22 and 24% at different

speeds and is influenced by the proportion of normal discharges and the efficiency of the crater overlaps. This metric adds depth to the understanding of continuous erosion dynamics, emphasizing the crucial role of discharge efficiency and spatial arrangements of craters.

This study offers insights into the assumption of MRR in the erosion process of cylindrical workpieces by comprehending the characteristics of single discharges. The findings, based on the studied material, can be applied in the conditioning of metal-bonded grinding wheels, where the bond material predominantly consists of bronze. Further investigations could simulate the impact of erosion parameters on the grinding wheel, taking into account the presence of non-conductive abrasive grains in the material.

Acknowledgements The authors would like to express their special thanks to Prof. Dr. Ing. Habil. Bastian E. Rapp, Department of Microsystems Engineering (IMTEK) at Albert-Ludwigs University of Freiburg and Mitsubishi Electric Company for valuable comments and support in knowledge and equipment throughout this project.

Author contribution Jahangir Khosravi: investigation, validation, roles/writing—original draft, writing—review and editing, methodology.

Hamid Hesni: investigation, conceptualization, methodology, analysis, roles/writing—original draft.

Bahman Azarhoushang: supervision, project administration, writing—review and editing, validation.

Declarations

Competing interests The authors declare no competing interests.

References

- Esteves PMB, Wiessner M, Costa JVMR, Sikora M, Wegener K (2021) WEDM single crater asymmetry. *Int J Adv Manuf Technol* 117(7):2421–2427. <https://doi.org/10.1007/s00170-021-07023-4>
- Klink A (2010) Wire electro discharge trueing and dressing of fine grinding wheels. *CIRP Ann* 59(1):235–238. <https://doi.org/10.1016/j.cirp.2010.03.076>
- Assarzadeh S, Ghoreishi M (2015) Electro-thermal-based finite element simulation and experimental validation of material removal in static gap single-spark die-sinking electro-discharge machining process. *Proc Inst Mech Eng Pt B J Eng Manufact* 231(1):28–47. <https://doi.org/10.1177/0954405415572661>
- Aspinwall DK, Soo SL, Berrisford AE, Walder G (2008) Workpiece surface roughness and integrity after WEDM of Ti–6Al–4V and Inconel 718 using minimum damage generator technology. *CIRP Ann* 57(1):187–190. <https://doi.org/10.1016/j.cirp.2008.03.054>
- Welschof L, Schäfer N, Herrig T, Klink A, Bergs T (2022) Effect of electrode material on removal efficiency regarding single discharges in wire EDM. *Int J Adv Manuf Technol* 120(3):1583–1589. <https://doi.org/10.1007/s00170-021-07858-x>
- Weingärtner E, Kuster F, Wegener K (2012) Modeling and simulation of electrical discharge machining. *Procedia CIRP* 2:74–78. <https://doi.org/10.1016/j.procir.2012.05.043>
- Wang Jun, Sánchez José Antonio, Izquierdo Borja, Ayesta Izaro (2020) Experimental and numerical study of crater volume in wire electrical discharge machining. *Materials* 13(3):577. <https://doi.org/10.3390/ma13030577>
- Yeo SH, Kurnia W, Tan PC (2008) Critical assessment and numerical comparison of electro-thermal models in EDM. *J Mater Process Technol* 203(1):241–251. <https://doi.org/10.1016/j.jmatprotec.2007.10.026>
- Sarathlal T P, Prabu Govindan (2021) A review on numerical modeling of electrical discharge machining. *Proceedings of the International Conference on Systems, Energy & Environment (ICSEE)*. <https://doi.org/10.2139/ssrn.3790346>
- Shahane S, Pande SS (2016) Development of a thermo-physical model for multi-spark wire EDM process. *Procedia Manufacturing* 5:205–219. <https://doi.org/10.1016/j.promfg.2016.08.019>
- Wang J, Sánchez JA, Izquierdo B, Ayesta I (2020) Influence of AISI D2 workpiece roughness on heat partition and plasma channel radius in the WEDM process. *Metals* 10(10):1360. <https://doi.org/10.3390/met10101360>
- Singh A, Ghosh A (1999) A thermo-electric model of material removal during electric discharge machining. *Int J Mach Tools Manuf* 39(4):669–682. [https://doi.org/10.1016/S0890-6955\(98\)00047-9](https://doi.org/10.1016/S0890-6955(98)00047-9)
- Haddad MJ, Fadaei Tehrani A (2008) Material removal rate (MRR) study in the cylindrical wire electrical discharge turning (CWEDT) process. *J Mater Process Technol* 199(1):369–378. <https://doi.org/10.1016/j.jmatprotec.2007.08.020>
- Gohil V, Puri YM (2015) Turning by electrical discharge machining: a review. *Proc Inst Mech Eng Pt B J Eng Manufact* 231(2):195–208. <https://doi.org/10.1177/0954405415590560>
- Rhoney BK, Shih AJ, Scattergood RO, Akemon JL, Gust DJ, Grant MB (2002) Wire electrical discharge machining of metal bond diamond wheels for ceramic grinding. *Int J Mach Tools Manuf* 42(12):1355–1362. [https://doi.org/10.1016/S0890-6955\(02\)00056-1](https://doi.org/10.1016/S0890-6955(02)00056-1)
- Weingärtner E, Wegener K, Kuster F (2012) Applying wire electrical discharge dressing (WEDD) to improve grinding performance of metal bounded diamond wheels. *Procedia CIRP* 1:365–370. <https://doi.org/10.1016/j.procir.2012.04.065>
- Khosravi J, Azarhoushang B, Zahedi A, Barmouz M (2023) Influence of wire electrical discharge conditioning on the grinding performance of metal-bonded diamond grinding tools. *Wear* 532–533:205080. <https://doi.org/10.1016/j.wear.2023.205080>
- Weingärtner E, Wegener K, Kuster F (2013) Influence of workpiece circumferential speed in wire electrical discharge machining. *Procedia CIRP* 6:238–243. <https://doi.org/10.1016/j.procir.2013.03.063>
- Uhlmann E, Piltz S, Jerzembeck S (2005) Micro-machining of cylindrical parts by electrical discharge grinding. *J Mater Process Technol* 160(1):15–23. <https://doi.org/10.1016/j.jmatprotec.2004.02.054>
- Bergs T, Schneider S, Harst S, Klink A (2019) Numerical simulation and validation of material loadings during electrical discharge machining. *Procedia CIRP* 82:14–19. <https://doi.org/10.1016/j.procir.2019.04.165>
- Hee Su Choe, Geon Woo Kim, Hyoung Kyu Cho, Goon Cheri Park, Kihak Im (2017) Effective heat capacity method with mesh adaptation for efficient simulation of phase change in the plasma facing wall of fusion demo reactor of fusion demo reactor, *Transactions of the Korean Nuclear Society Spring Meeting Jeju, Korea*
- Hinduja S, Kunieda M (2013) Modelling of ECM and EDM processes. *CIRP Ann* 62(2):775–797. <https://doi.org/10.1016/j.cirp.2013.05.011>

Publisher's Note Springer Nature remains neutral with regard to jurisdictional claims in published maps and institutional affiliations.

Springer Nature or its licensor (e.g. a society or other partner) holds exclusive rights to this article under a publishing agreement with the author(s) or other rightsholder(s); author self-archiving of the accepted manuscript version of this article is solely governed by the terms of such publishing agreement and applicable law.